#13

NOISE FIGURE OF TRAVELING-WAVE TUBES

CHARLES EDWARD MUEHE, JR.

TECHNICAL REPORT NO. 240

OCTOBER 16, 1952

RESEARCH LABORATORY OF ELECTRONICS
MASSACHUSETTS INSTITUTE OF TECHNOLOGY
CAMBRIDGE, MASSACHUSETTS

The Research Laboratory of Electronics is an interdepartmental laboratory of the Department of Electrical Engineering and the Department of Physics.

The research reported in this document was made possible in part by support extended the Massachusetts Institute of Technology, Research Laboratory of Electronics, jointly by the Army Signal Corps, the Navy Department (Office of Naval Research), and the Air Force (Air Materiel Command), under Signal Corps Contract DA36-039 sc-100, Project 8-102B-0; Department of the Army Project 3-99-10-022.

MASSACHUSETTS INSTITUTE OF TECHNOLOGY
RESEARCH LABORATORY OF ELECTRONICS

Technical Report No. 240 October 16, 1952

NOISE FIGURE OF TRAVELING-WAVE TUBES

Charles Edward Muehe, Jr.

This report is based on a thesis submitted to the
Department of Electrical Engineering, M. I. T.,
in partial fulfillment of the requirements
for the degree of Master of Science, August 1952.

Abstract

This report describes experiments primarily designed to measure the noise in electron beams and traveling-wave tubes at 3000 Mc/sec. Since it was desirable to know the dc conditions in the electron beam, the radial positive ion flow and the beam diameter were measured along the beam.

Measurement of the radial positive ion flow shows that the beam was fully neutralized by positive ions over all but a few centimeters of length near the anode. An analysis was made of the electron trajectories, and from measurements of beam shape the fact of full ion neutralization was confirmed.

With full ion neutralization there is considerable spiraling of the electrons and hence a dc velocity spread in a beam from a converging beam gun. For large magnetic fields this velocity spread causes an increase in the minima of the noise-current curve which is confirmed by experiment.

Next a double velocity jump was tried, since this is supposed to reduce the noise in the beam. It was found that the maxima of the noise-current curve could be reduced, but the minima were increased, and no success was achieved in reducing the noise figure of a traveling-wave tube with this device.

Finally, the noise current in an electron beam and the noise figure of a traveling-wave tube were measured under the same conditions; first with a converging beam electron gun, then with a parallel beam gun. The noise figures predicted from the noise-current curves agreed quite well when a correction was made for the nonzero minima of the noise-current curves. Finally, it was shown experimentally that a beam from a parallel beam gun is quieter than the same beam from a converging beam gun.

NOISE FIGURE OF TRAVELING-WAVE TUBES

I. Introduction

During the last few years a great deal of work has been done in trying to reduce the noise figure of traveling-wave tubes. This work has met with some success. D. A. Watkins (1) made a tube with a noise figure of 10 db by the use of a single velocity jump between the electron gun and the helix. R. W. Peter (2) has very recently announced a 9-db noise-figure tube made by experimentally adjusting the potential variation between cathode and anode for the lowest noise figure. These methods are essentially the same since the cathode-anode potential distribution in both is adjusted for minimum noise figure. Peter further reduced the noise figure to 8 db by lump loading the helix in order to increase the gain parameter C.

These are the only two methods that have been found successful in reducing the noise figure of a traveling-wave tube. Other methods tried have not met with success. The noise figure predicted for the tubes of Watkins and Peter is lower by a few decibels than the measured noise figure.

The experiments described in this report were performed in an effort to discover by experiment the important phenomena taking place in the tube. Since this is primarily a report on experimental work, the apparatus and procedure will be described in detail so that the resulting measurements may be evaluated more easily by the reader.

Description of the Apparatus

The apparatus used to measure the noise current in an electron beam and the noise figure of a traveling-wave tube is shown in Figs. 1 to 6.

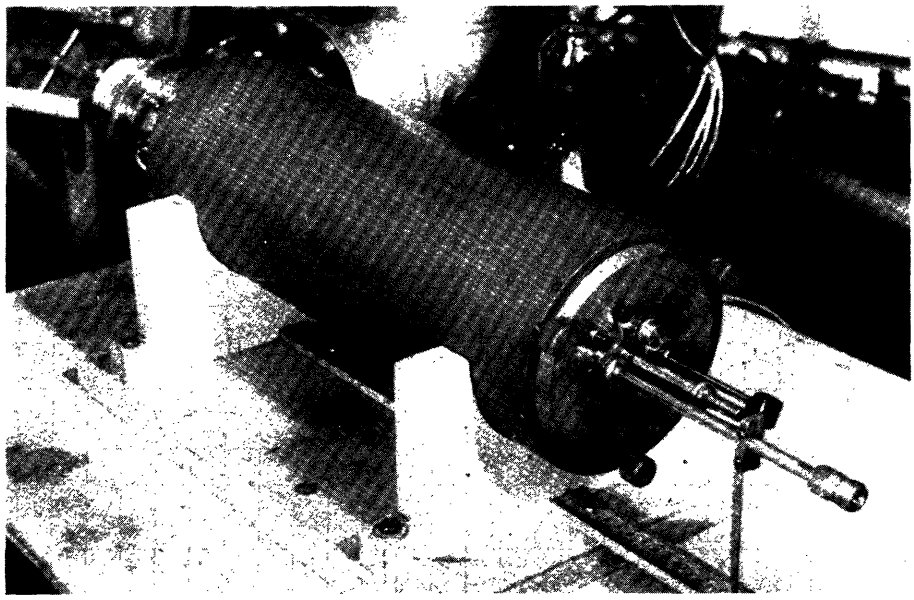

Fig. 1
Noise-measuring tube completely assembled.

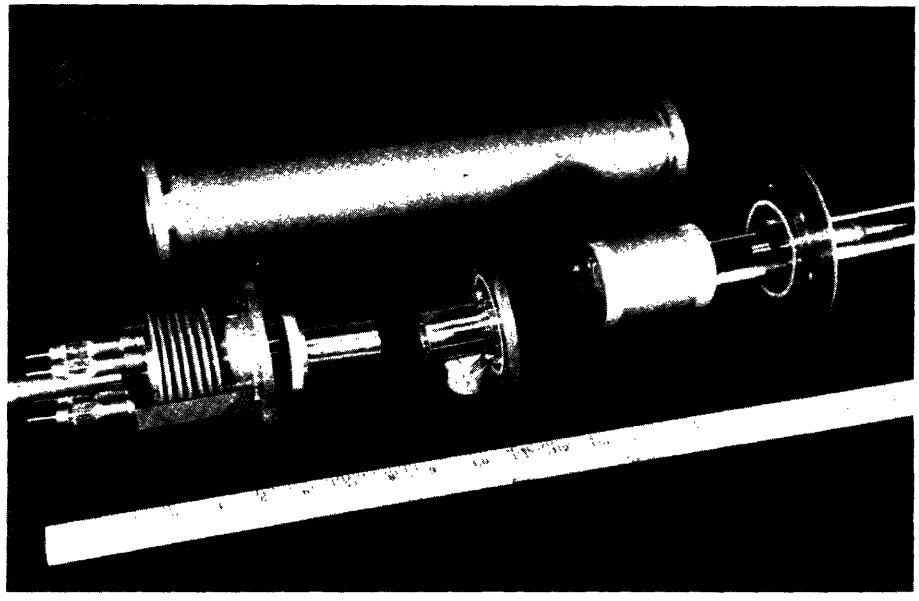

Fig. 2

Tube disassembled showing movable gun, shutter, cavity, and collector.

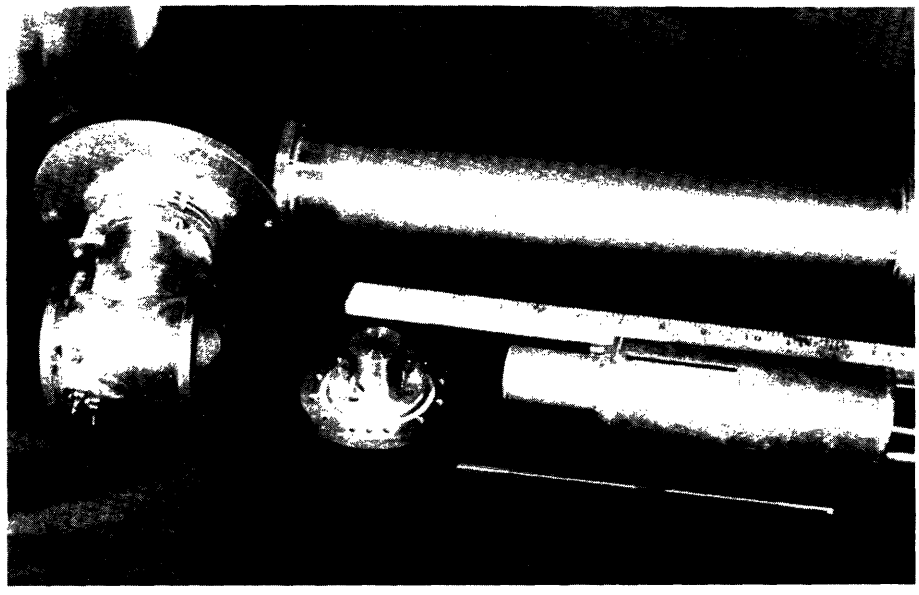

Fig. 3

Tube disassembled showing parallel beam gun, helix, and rf coupling units.

The beam in all cases was kept from diverging by a longitudinal magnetic field produced by the magnet shown in Fig. 1. Figure 7 shows the measured field along the axis of the magnet. Cooling was accomplished by forcing water from one end of the magnet to the other in approximately seven turns of quarter-inch copper tubing, then letting it flow back between the turns of the tubing, and removing it at the same end it entered. With this cooling no hot spots were observed and the magnet

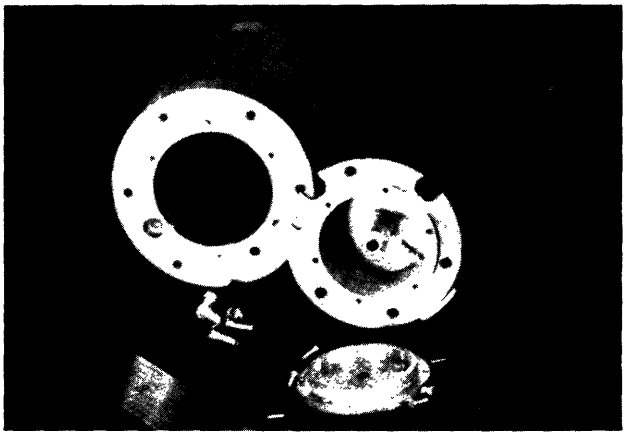

Fig. 4

Cavity disassembled.

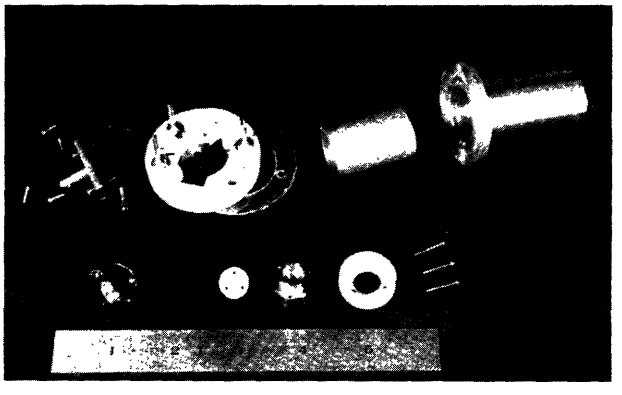

Fig. 5

Converging beam gun disassembled.

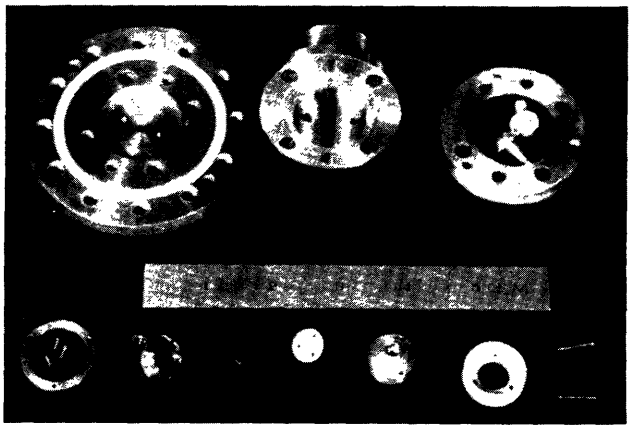

Fig. 6

Parallel beam gun disassembled.

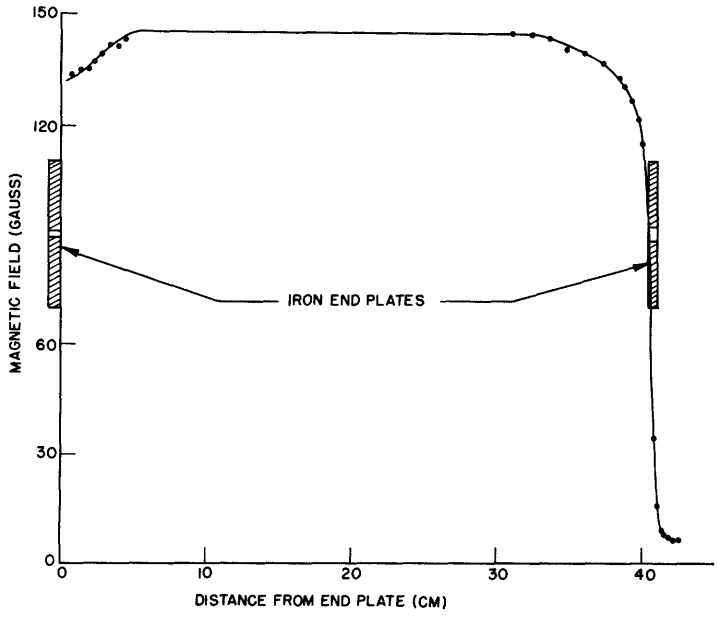

Fig. 7
Field on the axis of the magnet.

could be operated at 700 gauss for long periods of time. The magnet displayed no saturation effects up to a field of 850 gauss.

The main tube, shown in Figs. 2 and 3, was made of brass carefully honed to a perfectly round cylinder. It was chromium plated to provide a hard surface on which the movable brass cylinders could slide with ease. The iron end plates were carefully centered with respect to the main tube and held in place by dowel pins.

Two types of electron gun were used in the tube. The first type was a converging beam gun outside the magnetic field (Figs. 2 and 5). The second was a parallel beam gun immersed in the magnetic field (Figs. 3 and 6). With the apparatus shown in Fig. 2 the converging beam gun could be moved axially about three-quarters of an inch.

The cavity used to measure the noise current in the electron beam was of the re-entrant type. It resonated at approximately 3000 Mc/sec. The gap length was 0.060 inch, and the gap diameter was 0.120 inch. The center post of the cavity was recessed as shown in Fig. 4 to avoid capturing electrons between the cavity gap and the collector from a beam which varied in diameter along its length.

Figure 3 shows the helix with its associated coupling units. The helix was mounted in a piece of glass tubing. The glass tubing was supported in the coupling units, which were machined to slide easily in the main tube.

A hollow collector was used (see Figs. 1 and 2). It was placed at the end of the magnet, outside the magnetic field, so the beam would enter and spread to its inside walls. Secondary electrons are given off at all angles, but because of the depth of the collector, very few could find their way back out of it. Early in the experimental work it appeared that, because of an irregularity in the magnetic

field, some of the electrons were missing the collector and causing about 1 percent interception current. To remedy this situation, a funnel three-quarters of an inch in diameter was made and put on the end of the collector (Fig. 2).

With the tube in its final form, by proper positioning of the movable gun (when used), by the use of a small positive voltage on the collector, and by proper choice of magnetic field, the interception current could be reduced to a small negative quantity of 1 or 2 μa corresponding to the positive ion flow to the walls of the tube. Thus virtually 100 percent of the current could be transmitted to the collector.

Two different types of coaxial cables were used. The outer conductor of each type was made from a piece of brass tubing. The first type, shown in Fig. 2, had a dielectric and an inner conductor taken from a piece of RG-5/U cable. The inner conductor was extended to form the pick-up loop in the cavity. At the output end of the coaxial line a groove was cut into the dielectric to receive a small rubber O-Ring which provided the vacuum seal. The second type of coaxial line, shown in Fig. 3, used ceramic beads to hold the center conductor in place and had a kovar-to-glass vacuum seal at the output end.

All semipermanent O-Ring seals were made of Teflon. For the sliding seals at the end of the tube, rubber O-Rings were used because Teflon is not resilient enough to be used for an effective sliding vacuum seal.

The tube was exhausted with a four-inch metal diffusion pump. We used an inverted type of cold trap which held an eighteen-hour supply of liquid nitrogen. To prevent cathode poisoning, it was found necessary to keep liquid nitrogen in the cold trap at all times after the oxide-coated cathode was activated.

Two methods were used to measure the diameter of the beam. The first used the shutter shown in Fig. 2. It consists of a metal plate in which a series of various sized holes was drilled. The holes could be rotated in front of the beam. Given the percent of current through a given sized hole and assuming uniform current density in the beam, the beam diameter could be calculated. The second method used a piece of carbonized paper on which the beam fell. Being very thin, the carbon could not conduct much heat, so it was raised to a white heat where the electron beam hit it. The spot on the carbon target could be observed with a telescope and its diameter measured.

II. DC Conditions in the Electron Beam

In order to understand the ac or noise conditions in the beam, we must first understand the dc behavior of the beam. The essential dimensions of the two types of electron gun used in the experiments are shown in Fig. 8. The converging beam gun was designed by L. Stark at the Research Laboratory of Electronics. The parallel beam gun was a scaled-down model of one used by Watkins (1) and described in his report.

Distribution of Positive Ions

The converging beam gun was designed to operate under magnetically focused Brillouin flow (3) to produce an electron beam of uniform diameter. After a few experiments and as the result of a few

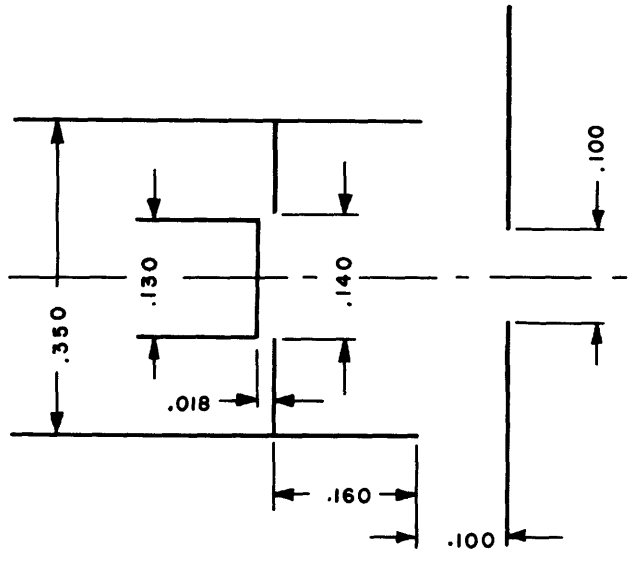

(a)

Fig. 8(a)

Essential dimensions of the converging beam electron gun.

perveance = 0.11×10^{-6} amp/volts$^{3/2}$

half angle = 7.2°; cathode arc radius = 0.530 inch; anode arc radius = 0.236 inch; beam diameter = 0.050 inch.

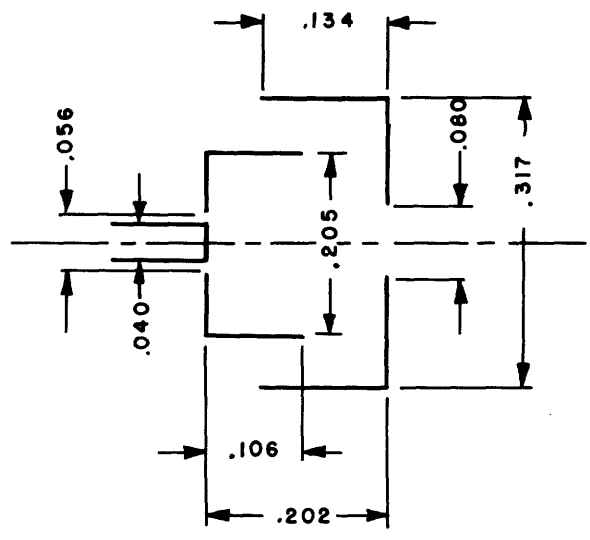

(b)

Fig. 8(b)

Essential dimensions of parallel beam electron gun.

perveance = 0.07×10^{-6} amp/volt$^{3/2}$.

simple considerations about the effect of positive ions in the beam, it was shown that this type of flow was impossible to attain in our tube.

At a pressure of 10^{-6} mm Hg and voltage of 1000 volts only one electron in 10,000 produces a positive ion in the 16-inch length of the tube. However, since these ions are produced with velocities of the order of only a hundredth of a volt, they quickly build up large space charges in the tube and their effect is far out of proportion to the small number produced per electron.

A satisfactory solution to the distribution of positive ions along an electron beam not confined by a magnetic field has been given by L. M. Field, K. Spangenberg, and R. Helm (4). Because of their great mass the ions are not greatly affected by the magnetic field if the beam diameter is small and we can use the above-mentioned solution. The solution is given in the form of a universal curve of positive ion space charge against distance as shown in Fig. 9, the equation of which, put in the rationalized mks system, is

$$\frac{3\pi}{2} n I_o \left[2\pi\epsilon\left(\frac{m^+}{e}\right)\right]^{1/2} (d - x) = (\rho_d^+ + 2\rho^+)(\rho_d^+ - \rho^+)^{1/2} \quad (1)$$

where n is the number of ions produced per electron per meter length of the beam, e is the charge of one ion or electron (1.60×10^{-19} coulomb), m^+ is the mass of one ion, d is the value of x where positive ion charge density has reached a maximum, ρ^+ is the linear positive ion charge density in coulombs per meter, ρ_d^+ is the maximum linear positive ion charge density in the beam, ϵ is the dielectric constant of free space, and I_o is the dc current in the beam.

For a short electron beam, d is at the collector, but if the beam is long enough, the latter portion of the beam will become fully neutralized and the positive ions will flow radially outward from the beam, in which case d is at the point where the electrons start flowing radially outward.

The position of the anode of the electron gun on the curve in Fig. 9 is fixed by the slope of the positive ion density curve at the anode. In the paper by Field, Spangenberg, and Helm (4), this slope is assumed proportional to the electric field leaking through the anode hole. We wish to find the distance from the anode to the point where the beam becomes fully neutralized. We shall not be far off, but a little optimistic, if we assume an infinite potential gradient at the anode, in which case the anode would lie at x, in Fig. 9.

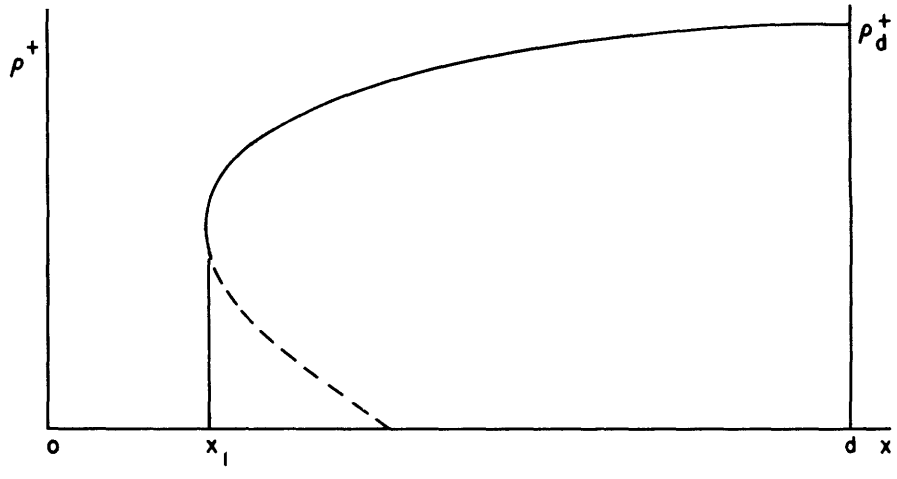

Fig. 9

Positive ion space charge density vs distance along the beam.

Differentiating Eq. 1 with respect to ρ^+ we have

$$\frac{3\pi}{2} n I_o \left[2\pi\epsilon \left(\frac{m^+}{e}\right)\right]^{1/2} \frac{dx}{d\rho^+} = \frac{3\rho^+ - \frac{3}{2}\rho_d^+}{(\rho_d^+ - \rho^+)^{1/2}} \qquad (2)$$

If we set this expression equal to zero, we find that

$$\rho_1^+ = \frac{1}{2}\rho_d^+ \qquad (3)$$

Substituting this value in Eq. 1 we have

$$\frac{3\pi}{2} n I_o \left[2\pi\epsilon\left(\frac{m^+}{e}\right)\right]^{1/2} (d - x_1) = (2)^{1/2} (\rho_d^+)^{3/2} \tag{4}$$

At x = d, however, the positive ion space charge is equal to the electron space charge; hence, if we set

$$\rho_d^+ = \frac{I_o}{\left[2\left(\frac{e}{m^-}\right) V_o\right]^{1/2}} \tag{5}$$

where V_o is the dc voltage of the beam and m^- is the mass of an electron, we find

$$Z_1 = d - x_1 = \frac{2}{3\pi \left(2\frac{e}{m^-}\right)^{1/4} \left(\frac{m^+}{m^-}\right)^{1/2} (2\pi\epsilon)^{1/2}} \frac{I_o^{1/2}}{n V_o^{3/4}} \tag{6}$$

Field, Spangenberg, and Helm (4) took the atomic weight of the molecule to be 16, assuming atomic oxygen. It is well known (5), however, that the main constituents of air form singly ionized molecules, the weight of nitrogen being 28 and that of oxygen 32. Since air is about three-quarters nitrogen and the ionization efficiency is almost identical for both gases, we have

$$\frac{m^+}{m^-} = 29 \times 1850 = 54{,}000 \tag{7}$$

Therefore Eq. 6 becomes

$$Z_1 = 0.159 \frac{I_o^{1/2}}{n V_o^{3/4}} \tag{8}$$

We now have a fairly good picture of the positive ion flow in the tube. Positive ions are formed uniformly throughout the cross section and length of the beam. They flow toward the center of the beam near the anode, and out through the anode hole, hit the cathode, and gradually destroy the material in a small spot at the center of the cathode. At a distance Z_1 from the cathode, given approximately by Eq. 8, the beam becomes fully neutralized and the ions start flowing radially toward the walls of the tube.

Experimental Verification of Ion Flow

To verify the conclusions as to the distribution of positive ions, an experiment was devised to measure the ions which flow radially out of the beam. A thin hollow cylinder slightly smaller in diameter than the tube was mounted so that it could be moved along the beam. Because of the large diameter (2 inches) of this cylinder, it was virtually impossible, in the magnetic field used, for any electrons to reach it. The cylinder was connected to the tube through a galvanometer with a resistance of approximately 250 ohms so that it was at the same potential as the tube.

The results are shown in Fig. 11. Because the cylinder was so long (4 inches), it collected ions over a considerable length of the tube. The positive ion current drops off for large values of Z because of the presence of an end plate. Some ions flow to the end plate instead of radially outward. At the beginning of the beam, however, there is a much larger drop in ion current; this is accounted for by the loss of ions through the anode hole.

Unfortunately, since the ion gauge used to measure the pressure was a considerable distance from the tube and partly isolated by a cold trap, it could give only a rough indication of the pressure in the tube. However, two days after the first ion measurements were taken, after the tube had plenty of time to outgas, the dotted curve shown in Fig. 11 was taken. Corresponding to the lower pressure, as indicated by the lower ion level, the action of the anode hole in removing ions from the first part of the beam is seen to extend over a greater distance.

We can check Eq. 8 against the dotted curve of Fig. 11. The measured value of ion current with −45 volts applied to the ion collector was 1.4 μa or 3.5 μa/m. If I^+ is the positive ion current per meter length of beam, then

$$n = \frac{I^+}{I_o} = \frac{3.5 \times 10^{-6}}{6 \times 10^{-3}} = 5.8 \times 10^{-4}$$

and

$$Z_1 = 0.12\,\text{m} = 12\,\text{cm}$$

As can be seen from Fig. 11, ions start to strike the walls of the tube approximately 13 cm from the anode.

Pressure in the Tube

So far the pressure in the tube has not come into our calculations. To put Eq. 8 in terms of pressure, we must know the rate n at which ions are produced. From the latest ionization data available to the author (5) the value of n for both nitrogen and oxygen for voltages above 500 volts may be written approximately as

$$n = \frac{3 \times 10^5 p}{V_o} \qquad (9)$$

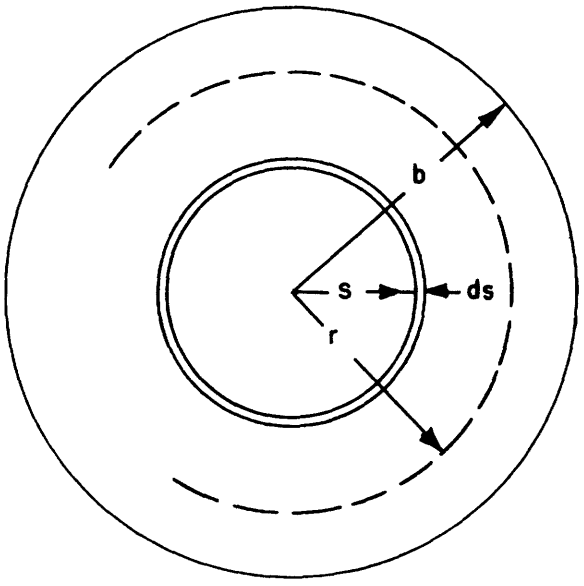

Fig. 10

Cross section of the beam.

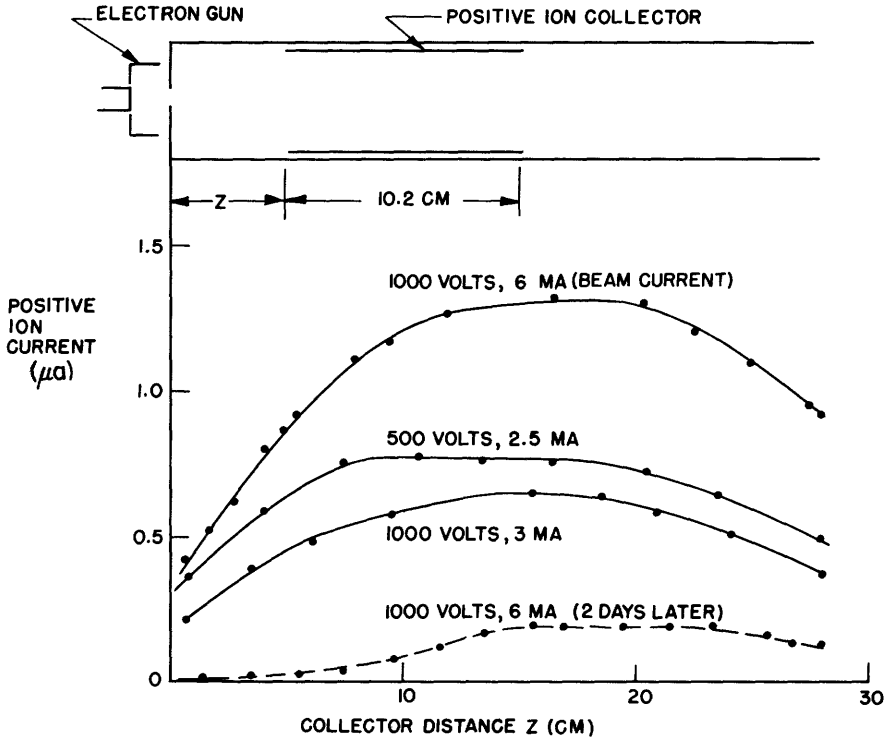

Fig. 11

Positive ion current as a function of the position of the ion collector along the beam.

where p is the pressure in mm Hg.

This is 20 times smaller than the expression given by Field, Spangenberg, and Helm (4). Substituting Eq. 9 into Eq. 8, we have

$$Z_1 = 5.3 \times 10^{-7} \frac{I_o^{1/2} V_o^{1/4}}{P} \tag{10}$$

Using the measured ion current, we can now also calculate the pressure

$$P = \frac{V_o n}{3 \times 10^5}$$

$$= 1.9 \times 10^{-6} \text{ mm Hg}$$

This value is about four times the pressure read on the ion gauge but is probably the correct pressure because of the distance between tube and ion gauge. Thus in all the experiments described in this report the true pressure was probably 1 to 2×10^{-6} mm Hg.

Potential Distribution in the Beam

The next question to be answered is: What is the radial potential distribution in the latter part of the beam necessary to drive the positive ions out toward the walls of the tube? Again we will neglect the magnetic forces. First, the potential depression in the beam caused by the negative electrons is filled up by positive ions. This would leave the beam neutral, except for the fact that positive ions continue to be produced and must create sufficient potential to drive themselves radially out of the beam. Figure 10 is a cross section of the beam.

Let dJ equal the positive ion current density at the radius r of the current which originated between the radii s and s + ds, and N equal the positive ion charge created per unit volume of the beam per second. Then

$$2\pi r\, dJ = N 2\pi s\, ds \tag{11}$$

If v_1 is the velocity of the current dJ when it crosses the radius and $d\rho$ represents its space charge density at this radius, then

$$d\rho = \frac{dJ}{v_1} = \frac{s\,ds}{r v_1} N \tag{12}$$

We also know that

$$v_1 = \left[2\frac{e}{m^+} [V(s) - V(r)]\right]^{1/2} \tag{13}$$

From Poisson's equation we have

$$\rho = - \epsilon \frac{1}{r} \frac{d}{dr} r \frac{dV}{dr} \tag{14}$$

Integrating Eq. 12 and combining it with Eqs. 13 and 14, we have

$$\int_o^r \frac{sN}{r \left[2 \frac{e}{m^+} [V(s) - V(r)]\right]^{1/2}} ds = - \epsilon \frac{1}{r} \frac{d}{dr} r \frac{dV}{dr} \tag{15}$$

to be solved under the following conditions at r = o, V = o, and dV/dr = o.

The solution is of the form

$$V = - Ar^2. \tag{16}$$

When this is put into Eq. 15 we find

$$A = \frac{N^{2/3}}{[4 \epsilon (2 \frac{e}{m})^{1/2}]^{2/3}} \tag{17}$$

Since the radial positive ion current per meter length of the beam I^+ can be measured, we can replace N by this quantity

$$N = \frac{I^+}{\pi b^2} \tag{18}$$

where b is the radius of the beam. Then Eq. 16 becomes

$$V = \left[\frac{I^+}{4 \pi \epsilon b^2 (2 \frac{e}{m^+})^{1/2}}\right]^{2/3} r^2 \tag{19}$$

The voltage between the center and the edge of the beam is

$$V_b = - 2.31 \times 10^4 (I^+ b)^{2/3} \tag{20}$$

For a typical case let I^+ equal 4×10^{-6} amp/m, b equal 0.025 inch = 6.35×10^{-4} m, and V_b equal – 0.043 volt. This is the order of magnitude of the voltage corresponding to the velocity of the ions when they are formed, so it requires practically no excess positive ion charge to drive the ions radially out of the beam once the electron charge has been fully neutralized.

To consider the effect of the magnetic field for a minute, look at the equation for the cutoff voltage of a magnetron with a vanishingly small cathode (3).

$$V_{co} = \frac{e}{m^+} \frac{(r_a B)^2}{8} = 4.27 \times 10^5 (r_a B)^2 \tag{21}$$

where r_a is the anode radius and B is the longitudinal magnetic field.

$$r_a = 0.026 \text{ inch} = 6.35 \times 10^{-4} \text{ m}$$
$$B = 0.070 \text{ webers/m}^2$$
$$V_{co} = 0.00083 \text{ volt.}$$

Since the cutoff voltage is much less than the initial voltage of the positive ions and much less than the voltage necessary to drive them out of the beam, we can safely state that the magnetic field does not affect the potential distribution within the beam caused by the positive ions in the beam.

Beam Shape for Converging Beam Gun

Now that we know the potential distribution in the beam, let us examine the electron trajectories to see what the beam shape will be like. The equation for radial motion of the electrons which originate from a gun outside the magnetic field is (ref. 3)

$$\ddot{r} - \eta \frac{dV}{dr} + \frac{\eta^2 B^2}{4} r = 0 \tag{22}$$

where $\eta = \frac{e}{m^-}$ and the dots indicate differentiation with respect to time.

We have seen that the latter part of the beam is almost exactly neutralized; we can therefore neglect the second term in Eq. 22 and obtain

$$\ddot{r} + \frac{\eta^2 B^2}{4} r = 0 \tag{23}$$

the solution of which is

$$r = A \cos \frac{\eta B}{2} t + B \sin \frac{\eta B}{2} t \tag{24}$$

The constants A and B are determined by the radius and slope at z = 0. They must be real numbers. It is easy to see that the electrons pass through the axis every half cycle. Let T be the length of time for a half cycle. Then

$$T = \frac{2\pi}{\eta B} \tag{25}$$

In measuring the beam diameter a minimum diameter will be observed at points along the beam separated by a distance corresponding to the transit time T. The observed wavelength should be

$$\lambda_c = u_o T = \frac{4\pi}{(2\eta)^{1/2}} \frac{V_o^{1/2}}{B} \tag{26}$$

If the beam were focused in Brillouin flow and slight perturbations existed due to imperfect starting conditions, the wavelength of these perturbations (3) would be

$$\lambda_b = 2^{1/2} \frac{4\pi}{(2\eta)^{1/2}} \frac{V_o^{1/2}}{B} \tag{27}$$

It is a simple matter to check experimentally the wavelength of the perturbations in the beam diameter. Four carefully measured cases are shown in Table I. First the beam diameter was measured along the beam using the shutter described earlier. The beam diameter vs distance curve was plotted, and the wavelengths were measured from the graph. The wavelength in the first few centimeters of the tube was slightly longer than in the rest of the beam in agreement with the fact that the beam was not fully neutralized for the first few centimeters of its length.

Table I

V_o	B	λ_c	Measured
(volts)	(gauss)	(cm)	Wavelength (cm)
1000	108	6.17	7.10
1500	198	4.12	4.66
1000	212	3.15	3.46
1000	353	1.89	1.94

Beam Shape for Parallel Beam Gun

In the case of the parallel beam gun immersed in the magnetic field, the equation for the radial motion of the electrons (3) is

$$\ddot{r} - \eta \frac{dV}{dr} + \frac{\eta^2 B^2}{4} r - \frac{\eta^2 B^2}{4} \frac{r_o^4}{r^3} = 0 \tag{28}$$

where r_o is the radius at the cathode. Again assuming the beam to be fully neutralized, we may drop the second term. Equation 28 then becomes

$$\ddot{r}_o + \frac{\eta^2 B^2}{4} r - \frac{\eta^2 B^2}{4} \frac{r_o^4}{r^3} = 0 \tag{29}$$

One solution is

$$r = r_o \tag{30}$$

However, since the first portion of the beam is not fully neutralized, initial conditions may not be correct to produce a parallel beam. Since Eq. 29 is nonlinear, we shall use the small perturbation theory to linearize it. Assume

$$r = a(1 + \alpha), \quad \alpha << 1 \tag{31}$$

Then Eq. 29 becomes

$$a\ddot{\alpha} + \frac{\eta^2 B^2}{4} a + \frac{\eta^2 B^2}{4} a\alpha - \frac{\eta^2 B^2}{4} \frac{r_o^4}{a^3} + \frac{\eta^2 B^2}{4} \frac{r_o^4}{a^3} 3\alpha = 0 \tag{32}$$

from which

$$a = r_o \tag{33}$$

The equation for the time-varying portion of r becomes

$$\ddot{\alpha} + \eta^2 B^2 \alpha = 0 \tag{34}$$

and the wavelength of the perturbations is

$$\lambda_c = \frac{2\pi u_o}{\eta B} = \frac{4\pi}{(2\eta)^{1/2}} \frac{V_o^{1/2}}{B} \tag{35}$$

This wavelength has been measured in only one case for the parallel beam gun. The result is shown in Table II.

Table II

V_o (volts)	B (gauss)	λ_c (cm)	Measured Wavelength (cm)
1000	310	2.15	2.40

It is interesting to observe that the wavelength in both types of flow is the same. There is a big difference in the actual flow of electrons in the two types, however. For the converging beam gun with full ion neutralization, the electrons go through the axis, whereas for the parallel beam gun the electrons are merely perturbed slightly from their equilibrium condition.

From this picture, it would be expected that the magnetic field required to confine a parallel beam is less than that required to confine a converging beam of the same size. This has been found to be true. Later we shall see how this difference in flow affects the noise in the beam.

III. Noise in Electron Beams and Traveling-Wave Tubes

The principal source of noise in an electron beam is shot noise, the random emission of electrons from the cathode. J. R. Pierce (14) has given us the simple theory used in most noise calculations. The electron gun used is always space-charge limited, so there is a reduction of noise due to space-charge smoothing at the potential minimum in front of the cathode. The shot noise is represented by an rms velocity modulation at the potential minimum. Pierce applies the infinite parallel plane diode equations of F. E. Llewellyn (6, 7) to obtain the current and velocity modulation at the anode. In a small frequency band these modulations are correlated and are 90° out of phase.

W. C. Hahn (8) and S. Ramo (9) have shown that, assuming the signals are small, a single velocity electron beam acts as a wave propagating structure. An infinite number of modes can be propagated, each with a different spatial field configuration. For each mode there are two waves, one with a velocity slightly greater than the average velocity and the other with a velocity slightly less than the average velocity of the electrons. In the simple theory given by Pierce only one of these modes, the one in which the longitudinal electric field is nearly constant over the cross section of the beam, is considered. The other modes may be important in determining the noise properties of electron beams, and they have been investigated by H. E. Rowe (15).

Pierce matches the velocity and current modulations at the anode of the electron gun to the two waves of the lowest mode given by Hahn and Ramo. Since the current and velocity modulations are 90° out of phase, both waves are excited equally, and an interference pattern of noise current or velocity appears along the beam. At successive points separated by half a plasma wavelength the noise current goes to zero, and at these same points the noise velocity modulation is a maximum. Thus the standing-wave ratio of the noise current measured along the beam, according to this simple theory, should be infinite.

Noise Experiments of Cutler and Quate

To check this simple theory experimentally C. C. Cutler and C. F. Quate (10) used an apparatus

very similar to the one described in Section I to measure the noise current in the electron beam. They found good agreement with theory except in two important respects. First they found that the distance from the anode to the first minimum was greater than that predicted by theory. This they attributed to the use of the infinite parallel plane equations of Llewellyn in the cathode-anode region when, in reality, the electron beam is far from being infinite in lateral extent. Second, they found that the noise current did not go to zero at the minimum but merely went down approximately 9 db below the noise-current maximum. This they attributed to partition noise caused by the interception of current before reaching the cavity. Their interception current was about 1 percent.

The first discrepancy found by Cutler and Quate has been overcome by the work of P. Parzen (11). In his work Parzen used a differential equation derived by L. D. Smullin (12) for infinite parallel plane flow. He modified this equation to take into account the finite size of the beam and then solved it approximately. The results put the minimum in its proper position.

The second discrepancy, that is, the absence of a real zero in the noise-current curve, was probably properly ascribed to partition noise in the experiments of Cutler and Quate. However, in the experiments to be described in this report the interception current has been reduced from 1 percent to below 0.1 percent. The minima in the noise-current curve were reduced slightly but did not approach zero.

Noise-Current Measurements in an Electron Beam

The noise-current curve measured by the cavity for a converging beam electron gun is shown in Fig. 12. The noise current is given in decibels below shot noise vs distance of the cavity from the anode. Since the cavity was connected to a 3000 Mc/sec receiver which gave only relative noise measurements, the cavity had to be calibrated. This was accomplished using the method described by Cutler and Quate (10). The heater voltage is reduced gradually, and at the same time collector current and noise output are read. When the heater voltage is low enough, the cathode becomes temperature limited and the noise output is directly proportional to the collector current. Then, knowing the noise output reading for pure shot noise at some small current, we can determine the full shot noise reading for any current, and calibrate the cavity.

Two precautions must be observed when calibrating a cavity in this manner: (a) The cavity must be as close to the anode as possible. Space-charge waves are initiated in the beam even by a temperature-limited gun, but next to the anode, full shot noise should be observed if the cathode is temperature limited. (b) The cavity calibration is different for different velocities of the electrons because the coupling coefficient of the cavity changes with velocity; hence, the cavity must be calibrated separately for every voltage used.

Another method was used to check the calibration of the cavity. The movable shutter was rotated in front of the cavity in order to intercept all but a small portion of the beam current. According to the theory of partition noise, the noise current should approach full shot noise as the current through the cavity approaches zero. The noise output was plotted vs the current allowed through the cavity, and a straight line with slope one was obtained for small currents. This method of cavity calibration agreed within 1.5 db with the previously described method. The partition noise method

suffers from the possibility of a false direct current reading. If a considerable number of secondary electrons, produced when the primary beam strikes the shutter, go through the cavity, the direct current will be increased; whereas the noise will not be altered because the secondary electrons have very low velocities and thus do not induce noise in the cavity. In agreement with this fact, the curves that have long straight parts of slope one for low currents agree very closely (within 0.5 db) with the curve taken by the temperature-limited gun method of calibration.

Returning to Fig. 12, the noise-current curve displays very well the standing-wave pattern except for small irregularities all along the curve. These irregularities are due to variations in the coupling coefficient of the cavity with variation in beam diameter. This is brought out very well by a careful inspection of Fig. 12. Under each small break in the noise-current curve, a maximum or minimum in beam diameter occurs. This variation in coupling coefficient with diameter of the beam limits the accuracy of all noise-current measurements to approximately 1 db.

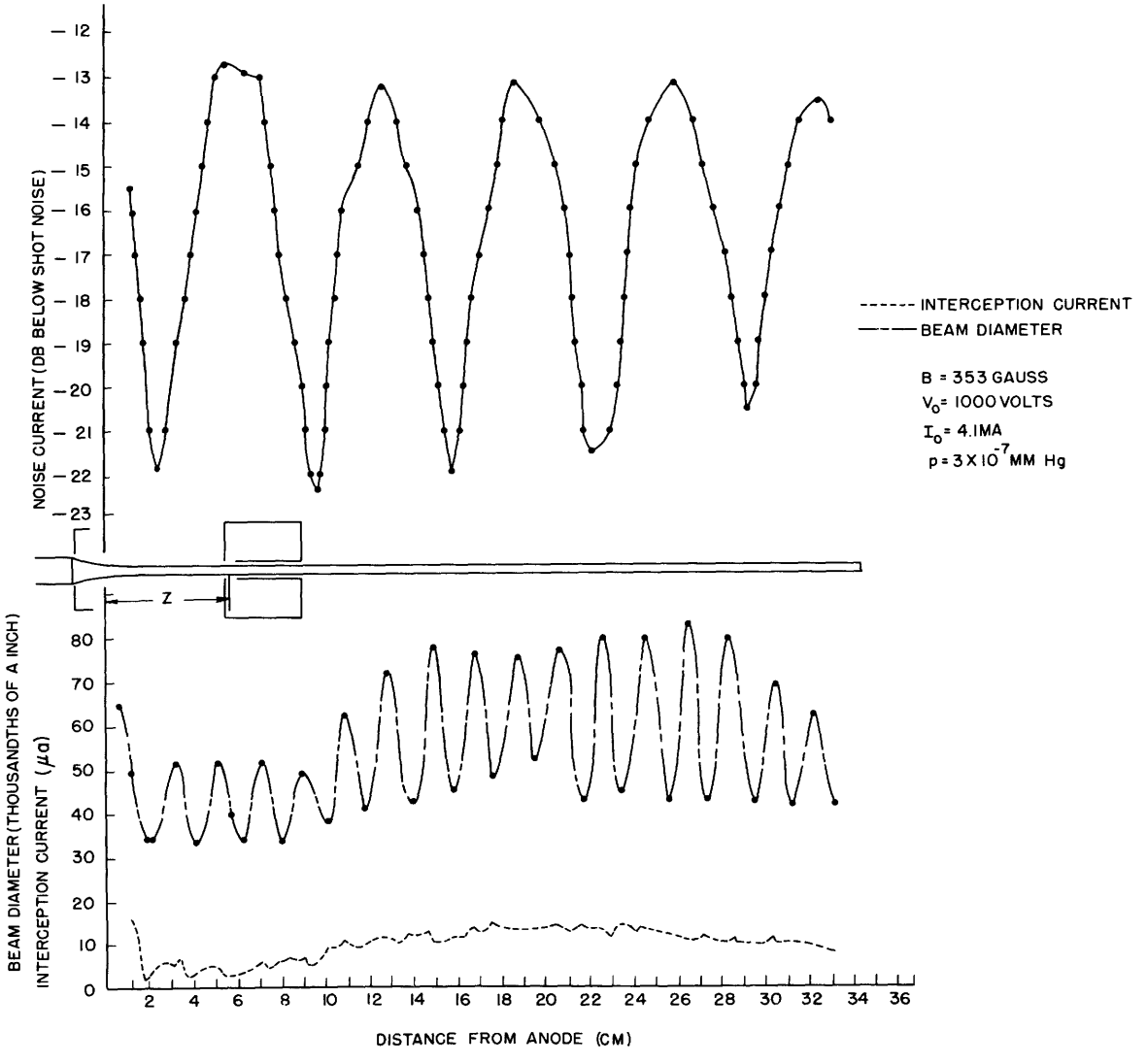

Fig. 12

Noise current, beam diameter, and interception current as a function of distance from the anode.

The Effect of Interception Current and Velocity Spread

Figures 13 and 14 show a very important aspect of the noise-current curve, namely, the variation of the maxima and minima or of the standing-wave ratio with magnetic field. Figure 13 shows the variation with magnetic field of the standing-wave ratio of noise current in a converging beam. Since the maxima of the noise-current curve changed very little, the variation in the standing-wave ratio is due mainly to variation in the minima. For small magnetic fields (less than 200 gauss) the decrease in the standing-wave ratio is due to the action of partition noise in raising the minima. For large magnetic fields, however, the standing-wave ratio was decreased because of increasing minima, and this cannot be blamed on partition noise because the interception current was very low. Compare this with Fig. 14 which shows the maxima and minima in a parallel beam immersed in the magnetic field as a function of magnetic field. We see that the standing-wave ratio is practically independent of magnetic field for all fields above approximately 100 gauss. The only logical explanation for these results seems to lie in the difference in the types of flow for electrons from a converging beam gun as compared to electrons from a parallel beam gun, as described in Section II. In the flow from a converging beam gun there is considerable spiraling of the electrons, and this spiraling increases with magnetic field, whereas for the parallel type of flow there is very little spiraling.

In the case of the converging beam gun the spiraling causes a dc velocity spread in the electron beam. The fully neutralized electron beam has the same potential throughout, so if we neglect the thermal velocities, all the electrons have the same linear velocity. However, the electrons at the edge of the beam spiral and pass through the axis of the beam every λ_c meters along the beam, whereas the electrons at the center of the beam go straight along the axis. Thus the fractional velocity spread is

$$\frac{a}{W} = \frac{1}{2}\left(\frac{\pi r_1}{\lambda_c}\right)^2 = \frac{n(r_1 B)^2}{16 V_o} \tag{36}$$

where: W is the linear velocity of all of the electrons, a is the difference in velocity in the z direction between electrons at the edge and those at the center of the beam, and r_1 is the maximum radius of the beam.

The standing-wave ratio to be expected with a given velocity spread has been worked out by H. A. Haus (13). He used for a model an infinite parallel-plane beam with the same type of dc velocity distribution as that caused by spiraling in an electron beam. For his noise input he considered a series of pulses and compensating pulses of current. A primary pulse in one velocity group is accompanied by a compensating fluctuation in all other velocity groups, coherent with it and 180° out of phase. There are primary pulses in all velocity groups, and these are uncorrelated. The compensating fluctuations are just sufficient to produce a noise current Γ below full shot noise. He took full account of space charge and found that for small velocity spread a standing wave of noise current should be measured in the beam with a standing-wave ratio of

$$SWR = 12\left(\frac{W}{a}\,\Gamma\,\frac{\omega_p}{\omega}\right)^2 \tag{37}$$

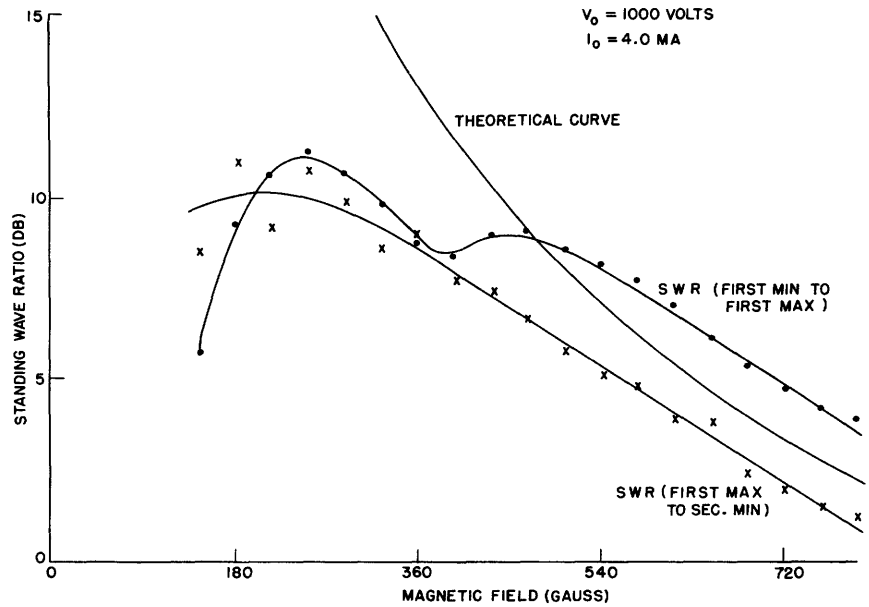

Fig. 13

Standing-wave ratio vs magnetic field for converging beam gun.

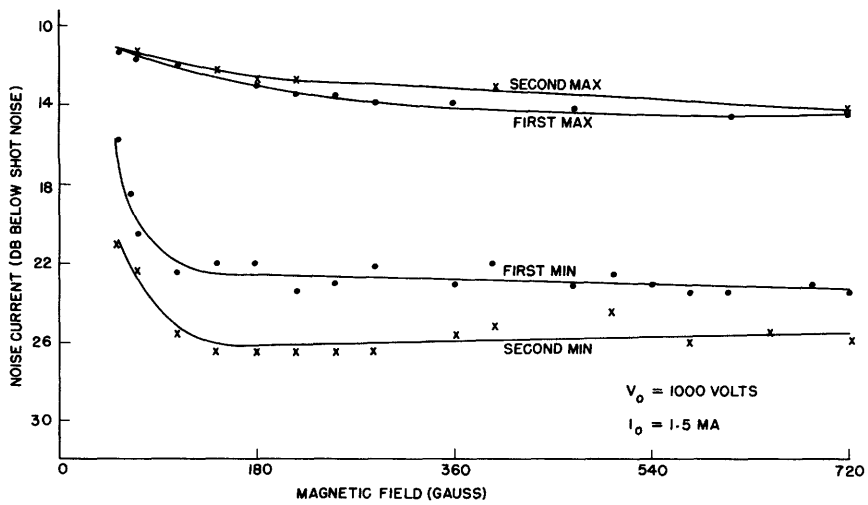

Fig. 14

Noise-current maxima and minima for the parallel beam gun.

where ω_p is the plasma frequency, and ω is the radian frequency at which noise is being measured.

In order to apply this to the finite beam actually measured, we used the measured plasma frequency to correct for the finite dimensions of the beam, and for Γ we used the measured value of the maximum of the noise-current curve below full shot noise. The calculated curve is shown in Fig. 13. It agrees fairly well with the measured standing-wave-ratio curves for magnetic fields above approximately 400 gauss and shows that in this region the dc velocity spread determines the noise-current minima. Contrast this with Fig. 14 for a parallel gun in which there is practically no spiraling of the electrons. The standing-wave ratio is almost independent of the magnetic field.

This still leaves unexplained the nonzero minima in the noise-current curve shown by the finite standing-wave-ratio curve in Fig. 13 in the range of 200 and 400 gauss, and the entire minima curve in Fig. 14.

The remainder of the noise experiments described in this section were performed in an effort to shed some light on these so far unexplained phenomena.

Chu's Equivalent Transmission Line Theory

The remaining experiments will be explained in terms of L. J. Chu's equivalent transmission line theory of an electron beam. Briefly his theory is as follows. Consider the flow of electrons past a given plane in the beam. The electrons are flowing in the $+z$ direction. Each electron carries a kinetic energy of $\frac{1}{2}(mv_z^2)$ and there are $(-I/e)$ electrons in the beam, where I is the current in the beam.

Then the kinetic power in the beam may be written

$$P = -\frac{mv_z^2}{2}\ \frac{I}{e} = -I \cdot \frac{mv_z^2}{2e} \tag{38}$$

We see at once that $(mv_z^2/2e)$ has the dimensions of a voltage. Now if we assume that the small signal theory applies, we may write

$$I = -I_o + i \exp(j\omega t) \tag{39}$$

$$\frac{mv_z^2}{2e} = V_o + V \exp(j\omega t) \tag{40}$$

$$v_z = u_o + v \exp(j\omega t) \tag{41}$$

Neglecting double frequency terms, we have

$$v_z^2 = u_o^2 + 2u_o v \exp(j\omega t) \tag{42}$$

Combining Eqs. 40 and 42, we can state

$$V = \frac{mu_o v}{2e} \tag{43}$$

$$V_o = \frac{mu_o^2}{2e} \tag{44}$$

Let us assume that the beam is propagating only one mode. Then, according to Ramo (9), the ac velocity and current may be written

$$v = (v^+ \exp(-j\delta z) + v^- \exp(j\delta z) \exp[j(\omega t - \beta_e z)] \tag{45}$$

$$i = -\frac{\rho_o \omega}{\omega_q}(v^+ \exp(-j\delta z) - v^- \exp(j\delta z) \exp[j(\omega t - \beta_e z)] \tag{46}$$

where δ equals ω_q/u_o, β_e equals ω/u_o, and ω_q is the effective plasma radian frequency. Using Eqs. 43 and 44 and dropping the $\exp[j(\omega t - \beta_e z)]$ part, we find

$$V = V^+ \exp(-j\delta z) + V^- \exp(j\delta z) \tag{47}$$

$$i = \frac{1}{Z_o}(V^+ \exp(-j\delta z) - V^- \exp(j\delta z) \tag{48}$$

where

$$Z_o = \tfrac{1}{2}\frac{V_o}{I_o}\frac{\omega_q}{\omega} \tag{49}$$

and the time average kinetic power carried by the beam is

$$P_k = I_o V_o - \frac{iV^*}{2} \tag{50}$$

$$= I_o V_o - \frac{|V^+|^2}{2Z_o} + \frac{|V^-|^2}{2Z_o}$$

The first term is the dc power which is always positive. The second and third terms represent the ac power. If the wave traveling slightly slower than the average velocity of the electrons is excited more strongly than the wave traveling slightly faster than the average velocity, the ac power is positive, whereas if the reverse is true, the ac power is negative. The total power is always positive, however, because of the small signal approximations made at the beginning of this argument.

Velocity-Jump Experiment

The first experiment to be described is a velocity-jump experiment. In this experiment the electrons originally traveling at some high velocity (1000 volts) are suddenly reduced in velocity to some low velocity (250 volts). They are allowed to drift for a portion of a plasma wavelength at this low velocity and then suddenly are brought back to their original velocity. The noise is measured in the electron stream before and after the velocity jump.

Since Eqs. (47) and (48) for the ac voltage and current in the beam are the same as the equations for voltage and current on a transmission line, a Smith chart may be used to calculate the current after a velocity jump. First, however, one must know the effective length of the velocity-jump section. This is not the same as the actual length because the velocity jumps do not occur in an infinitely short distance. The effective length of the velocity-jump section is measured as indicated in Fig. 15. The first velocity-jump section is placed at a noise-current maximum, and the cavity is placed either one-fourth or one-half wavelength from the second velocity jump. Then as the voltage of the center part of the velocity-jump section is varied, the curves of Fig. 15 are obtained. The maxima and minima indicate the voltages at which the velocity-jump section is a multiple of a quarter wavelength long. These are marked in Fig. 15.

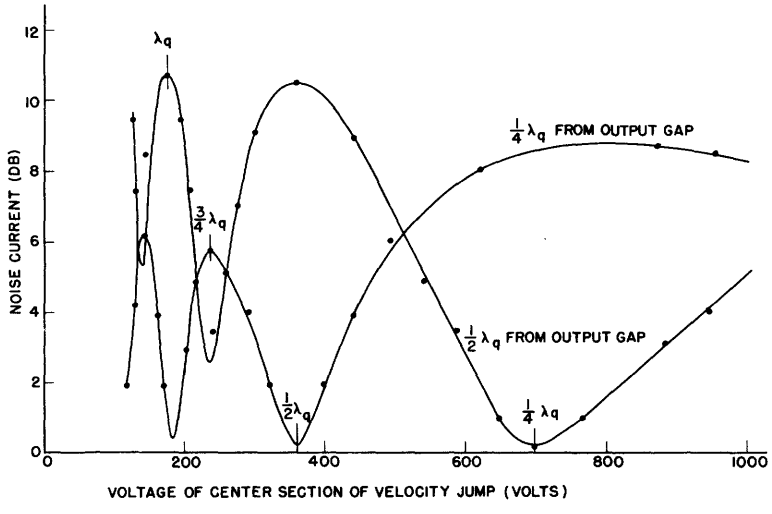

Fig. 15

Noise current at distances of ¼(λ_q) and ½(λ_q) from second velocity jump vs voltage of center part of velocity-jump section.

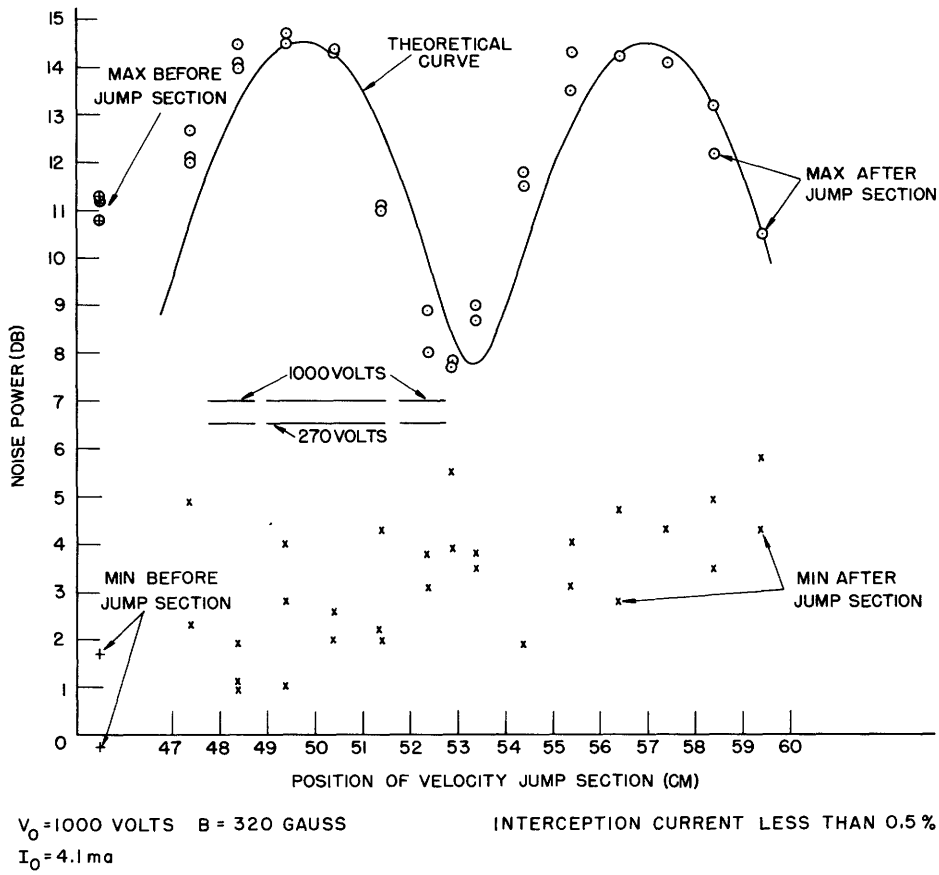

Fig. 16
First velocity-jump experiment.

Figures 16 and 17 show the result of an experiment to test the effectiveness of a velocity-jump section. The velocity-jump section was held at a constant voltage. It was moved along the beam, and the maxima and minima of the noise current were measured after the jump section and plotted as a function of the distance of the jump section along the beam. In Fig. 16 the minima were quite badly scattered, so the theoretical curve for the maxima was calculated on the basis of an infinite standing-wave ratio before the velocity-jump section. The interception current in this case was kept less than 0.5 percent. The experiment was repeated (see Fig. 17), the interception current being kept at less than 0.1 percent. The theoretical minima and maxima were calculated using a Smith chart, and the measured minima and maxima were calculated before the velocity-jump section. The assumption of kinetic power conservation in the beam was used to obtain the absolute levels for the calculated curves. The maxima agree very well with theory, but the minima, although showing a definite rise where the maxima were the lowest, do not agree very well with this theory. The reason for the measured values of the minima is not understood at this time.

Noise-Figure Experiments

The last two experiments, the results of which are shown in Figs. 18 and 19, are the most directly connected with the subject of this report. In these experiments the noise figure of a traveling-wave

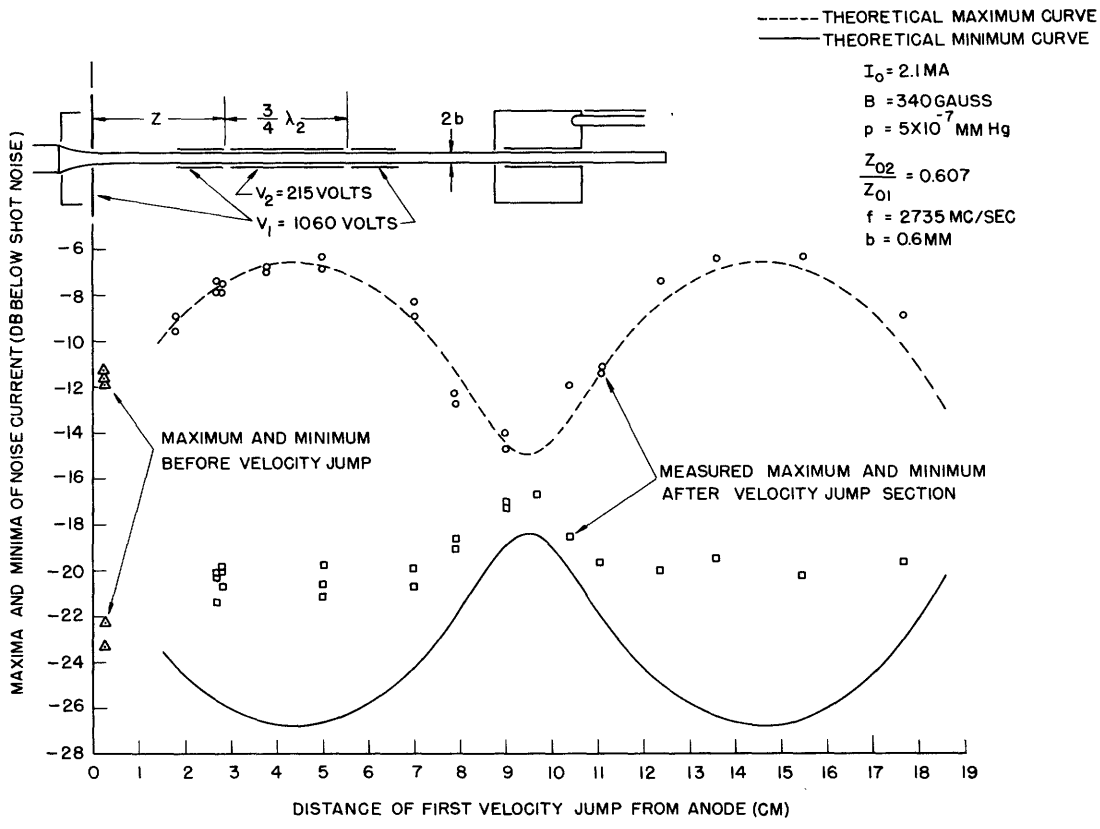

Fig. 17
Second velocity-jump experiment.

tube was measured under the same conditions as those which existed for the noise-current measurements. The noise figure and noise current were measured by using two different kinds of electron guns giving almost the same dc beam conditions.

The helix was 0.100 inch in inside diameter, 5.75 inches long, and wound with 0.005-inch tungsten wire with a pitch of 0.027 inch. It was supported in a piece of Pyrex tubing. To find the noise figure of a traveling-wave tube, Pierce (14) matched the noise current and velocity in the electron beam, calculated as described earlier in this section, to the three forward waves in the helix and found the magnitude of the growing wave arising from the noise in the electron beam. He then found the thermal noise in the helix matched to a source at room temperature, and comparing the two noises, found the noise figure of the helix. Pierce's calculations were limited to the case of zero loss and zero space charge. D. A. Watkins (1) extended this analysis to cover arbitrary values of the space-charge parameter QC and the loss parameter d. In the appendix Watkins' curves have been recalculated for closer values of d and QC, along with the calculation of the growing root of Pierce's cubic equation. In his paper Watkins finds the following expression for the noise figure of a traveling-wave tube

$$F = 1 + \frac{I_o}{2\eta CkT\Delta f}\left[(\delta_2 + \delta_3)\,v + \frac{u_o C}{jI_o}\,(\delta_2\delta_3 - 4QC)\,i\right]^2 \qquad (51)$$

He assumed an infinite noise standing-wave ratio in the beam preceding the helix.

$$i = -\,j\,v_m\,\frac{\omega}{\omega_q}\frac{I_o}{u_o}\,\sin\,\delta z \tag{52}$$

$$v = v_m\,\cos\,\delta z \tag{53}$$

Putting Eqs. 52 and 53 into Eq. 51, he found

$$F = 1 + \frac{I_o v_m{}^2}{2\eta CkT\Delta f}\,f(QC, d, \delta z) \tag{54}$$

where

$$f(QC, d, \delta z) = \left|(\delta_2 + \delta_3)\,\cos\,\delta z - \frac{\delta_2\delta_3 - 4QC}{(4QC)^{1/2}}\,\sin\,\delta z\right|^2 \tag{55}$$

Now if the standing-wave ratio of noise current in the beam is not infinite because of the excitation of one wave in the beam more than the other, we may express the velocity and current modulation as

$$v = v_{max}\,\cos\,\delta z \mp j\,v_{min}\,\sin\,\delta z \tag{56}$$

$$i = -\,j\,\frac{\omega I_o}{\omega_q u_o}\,(v_{max}\,\sin\,\delta z \mp j\,v_{min}\cos\,\delta z) \tag{57}$$

To show the meaning of these expressions we expand Eq. 56 and derive

$$\begin{aligned} v = {} & \tfrac{1}{2}\,(v_{max} \mp v_{min})\exp\,(-j\delta z) \\ & + \tfrac{1}{2}\,(v_{max} \pm v_{min})\,\exp\,(+j\delta z) \end{aligned} \tag{58}$$

If the top sign is used, the wave traveling slower than the average velocity of the electrons is the larger, and there is positive ac power in the beam. If the bottom sign is used, there is negative ac power in the beam.

If we put Eqs. 56 and 57 into Eq. 51, we find a new function f(QC, d, δz). The new maximum and minimum values of this function become

$$f'_{min} = [\, f_{min}^{1/2} \pm \rho\, f_{max}^{1/2} \,]^2 \tag{59}$$

$$f'_{max} = [\, f_{max}^{1/2} \pm \rho\, f_{min}^{1/2} \,]^2 \tag{60}$$

where f_{max} and f_{min} are the maximum and minimum values of Eq. 55 calculated on the basis of an infinite standing-wave ratio in the beam and

$$\rho = \frac{v_{min}}{v_{max}} = \frac{1}{VSWR} \tag{61}$$

Now, to put Eq. 54 into a form which may be more readily applied, we may use the relation

$$i_m^2 = v_m^2 \left(\frac{\omega I_o}{\omega_q u_o} \right)^2 \tag{62}$$

where i_m is the noise current at a maximum in the noise-current curve. If we define

$$\Gamma_m^2 = \frac{i_m^2}{2eI_o \Delta f} \tag{63}$$

Eq. 54 becomes

$$F = 1 + \frac{\omega_q^2 u_o^2 \Gamma_m^2 e}{\omega^2 \eta CkT} f(QC, d, \delta z) \tag{64}$$

Assuming T = 290°K, we find that the noise-figure expression becomes

$$F = 1 + 2.81 \times 10^{13} \frac{V_o^2 \Gamma_m^2}{\lambda_q f^2 C} f(QC, d, \delta z) \tag{65}$$

All of the necessary quantities to calculate F can be measured with the exception of C and Q. In calculating the impedance of the helix, needed to calculate C, a correction had to be made for the

effect of the glass dielectric used to support the helix. The phase velocity v_p and the impedance K_s were calculated for a helix in space from the curves in Pierce's book. The effect of the surrounding glass tube was accounted for by using the measured phase velocity u_o, and the true impedance K was calculated by using the equation

$$K = \frac{u_o}{v_p}\left[\frac{I_o(\frac{\omega}{v_p}a)}{I_o(\frac{\omega}{u_o}a)}\right]^2 K_s \tag{66}$$

This equation is derived in Pierce's text (see ref. 14, p. 44). C was then calculated with the corrected value of K, and Q was calculated from the relation

$$4QC^3 = \left(\frac{\omega_q}{\omega}\right)^2 \tag{67}$$

from which

$$Q = \frac{1}{4C^3}\left(\frac{u_o}{f\lambda_q}\right)^2 \tag{68}$$

The loss was added to the helix by depositing nickel on a short section near the center on the inside of the glass tube used to support the helix. A heavy loss was added so the helix was essentially severed in this section. We then calculated the gain, using the data in reference 14, chapter IX, where Pierce gives the loss of the growing wave in a severed section of the helix. The measured gain was within 2 db of the calculated gain for all beam currents at which there was any gain. Thus the values of Q and C are probably quite accurate.

The noise experiments, the results of which are shown in Figs. 18 and 19, were performed in the following manner. First, the helix with its associated coupling units was put in the tube, the tube exhausted, and the noise figure vs distance curve taken. Next, dry nitrogen was admitted into the tube, the helix removed and the cavity put in its place. The tube was again exhausted, and the noise current vs distance curve was taken. Then the cavity was calibrated as described earlier in this section. An attempt was made using the converging beam gun to reduce the noise figure with the double velocity-jump section described earlier, but we were never successful in reducing the noise figure below that obtained without the velocity-jump section. In Fig. 19 a theoretical noise-current curve is shown. It was calculated using the results of Parzen (11) and is seen to agree quite well except for the minima which should go to minus infinity decibels.

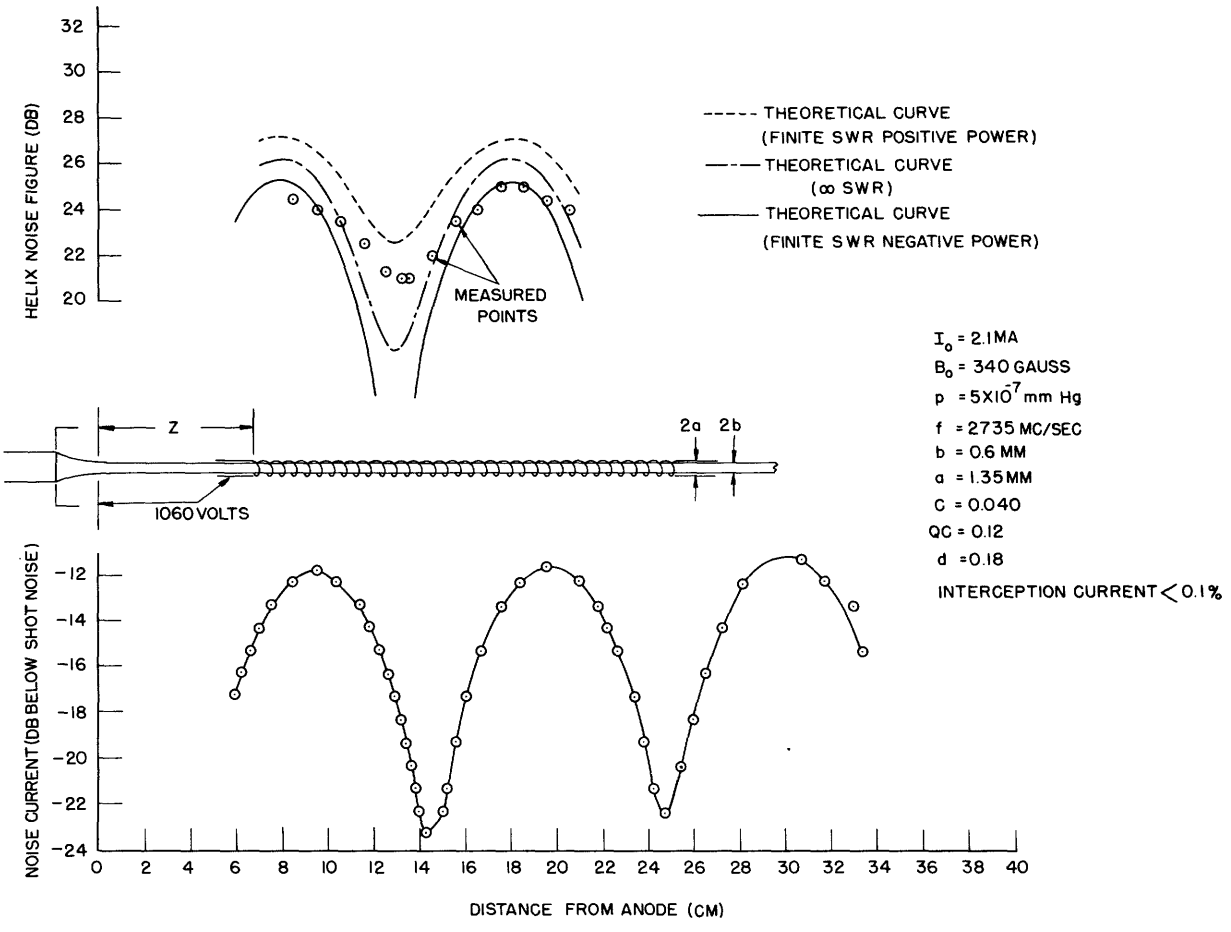

Fig. 18

Noise current and noise figure using converging beam gun.

The noise-figure curves were calculated using Eq. 65. In Fig. 18 the correction for a finite standing-wave ratio, given by Eqs. 59 and 60, was made for both positive and negative power in the beam. In Fig. 19 only the correction for positive power was made.

An important thing to notice in comparing Figs. 18 and 19 is that for the parallel beam gun both the noise figure and the noise current are 3.5 to 4 db below those of the converging beam gun.

Conclusions

A number of interesting facts have been brought out by these experiments. The fact that the beam is almost fully neutralized in our tube leads to a difference in the type of flow between a beam from a converging beam gun and one from a parallel beam gun. This difference in flow causes a velocity spread in the converging gun case so that the noise-current minima for large magnetic fields is increased.

Further, it was shown that a double velocity jump, while decreasing the maxima in the noise-standing wave, at the same time increased the minima, and this action somehow prevents the reduction of the noise figure of a helix.

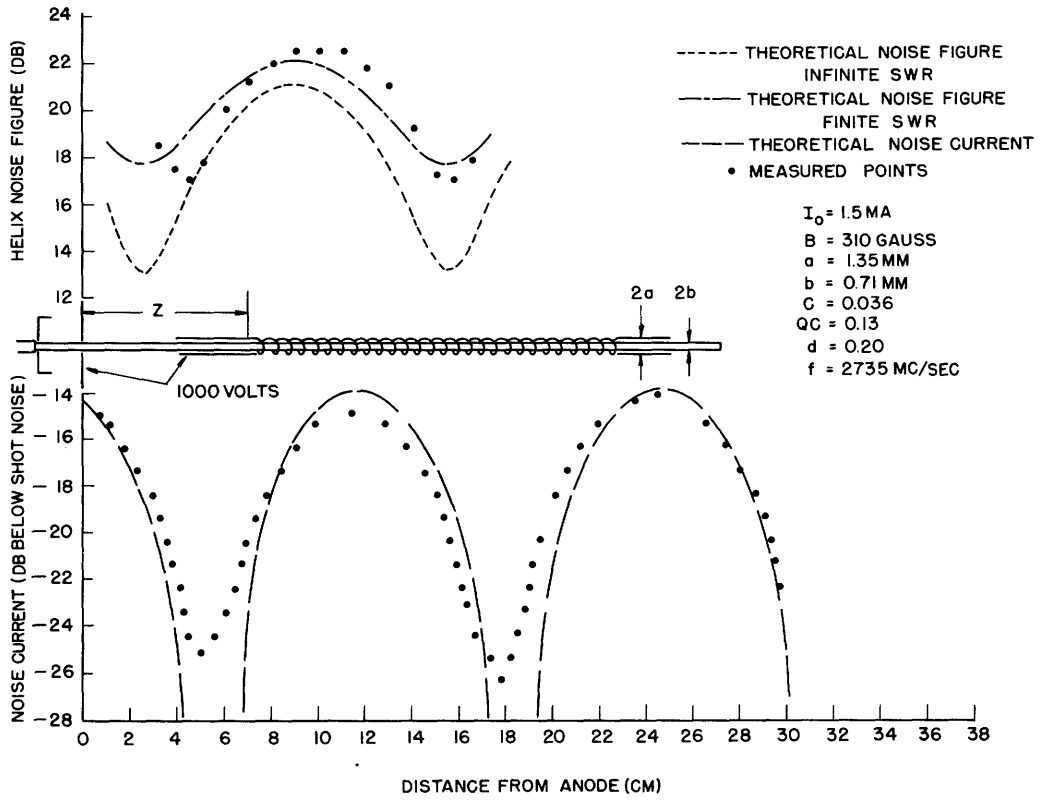

Fig. 19

Noise current and noise figure using parallel beam gun.

The noise figure and noise current have been measured for a converging beam and parallel beam gun, and the noise figure checks quite well when a correction is made for the finite noise current minima. The parallel beam gun is less noisy by approximately 4 db than the converging beam gun.

In conclusion, it should be pointed out that the present theory to explain the noise experiments with velocity jumps and helix is used only for simplicity. The assumption of a single velocity beam propagating only one mode whose two waves are excited unequally is only a crude approximation of the actual situation. At the present time no other theory, except the multivelocity theory which was shown not to apply, has been developed sufficiently for a direct application to these problems. It is hoped that in the near future a more satisfactory theory will be worked out.

APPENDIX

Solution of Pierce's Cubic Equation

In his book Pierce gives the following cubic equation which, when solved, will yield the propagation constants of the three forward waves in the traveling-wave tube.

$$\delta^2 = \frac{1}{(-b + jd + j\delta)} - 4QC \tag{A.1}$$

We wish to find the roots of this equation under the condition that the real part of one of the roots (δ_1) be a maximum with respect to the velocity parameter b. This is the condition in which the electron velocity is adjusted for maximum gain.

Differentiating Eq. A.1 with respect to b we have

$$\frac{d\delta}{db} = \frac{1}{j + 2\delta(-b + jd + j\delta)^2} \tag{A.2}$$

Let

$$\delta = x + jy \tag{A.3}$$

If we put Eq A.3 into Eq. A.2, separate out the real part, and set it equal to zero, we have

$$x(b + y)^2 - x(d + x)^2 + 2y(b + y)(d + x) = 0 \tag{A.4}$$

If we put Eq. A.3 into Eq. A.1 and separate into real and imaginary parts, we obtain the two equations

$$x^3 - 3xy^2 + dx^2 - dy^2 - 2bxy + 4QCx + 4QCd = 0 \tag{A.5}$$

$$3x^2y - y^3 + 2dxy + bx^2 - by^2 + 4QCy + 4QCb + 1 = 0 \tag{A.6}$$

We must now solve Eqs.A.4, A.5, and A.6 simultaneously for x and y as a function of QC and d and at the same time eliminate b. To do this in a straightforward manner would involve the solution of complicated higher-order equations. Therefore, the equations were solved for the parameters in terms of the unknown roots, and the following equations were obtained

$$QC = \frac{1}{4}\left[-2y_1 (x_1^2 + y_1^2)^{1/2} - (x_1^2 + y_1^2)\right] \tag{A.7}$$

$$d = -x_1 - \frac{1}{4x_1 y_1} + \frac{1}{4x_1 (x_1^2 + y_1^2)^{1/2}} \tag{A.8}$$

$$b = -y_1 + \frac{1}{4y_1 (x_1^2 + y_1^2)^{1/2}} \tag{A.9}$$

Figures A.1 and A.2 show the values of x_1 and y_1, found by using these equations.

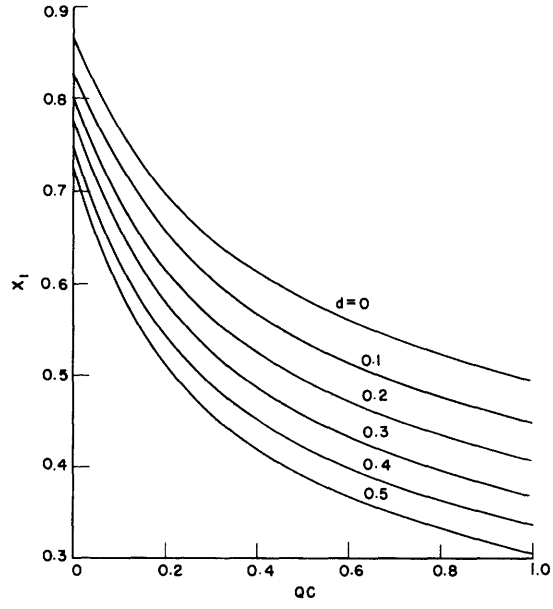

Fig. A.1
Graph of x_1 vs QC with d as parameter.

We are now in a position to calculate the gain of a traveling-wave tube with uniform loss more accurately than the method used by Pierce in Appendix 7 of his book. The gain is given by

$$G = A + BCN \tag{A.10}$$

Instead of correcting for the loss as prescribed by Pierce, we find the correct value of B by using Fig. A.1 and the equation

$$B = 54.5 x_1 \tag{A.11}$$

To find the other two roots of Eq. A.1 we divide this equation by $\delta - \delta_1$ to eliminate the first root and obtain

$$\delta^2 + (\delta_1 + d + jb)\,\delta + \delta_1 (\delta_1 + d + jb) + 4QC = 0 \tag{A.12}$$

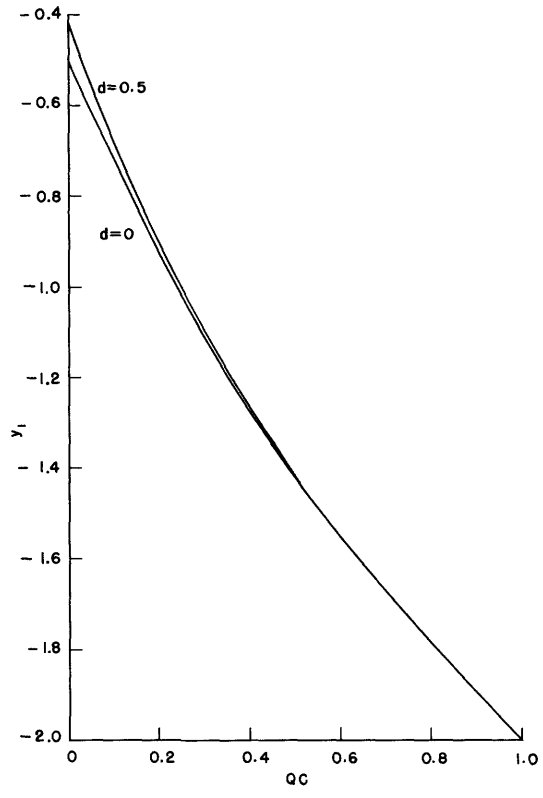

Fig. A.2
Graph of y_1 vs QC with d as parameter.

We are interested in the other two roots only as they are found in Watkins' expression

$$f(QC, d, \delta z) = \left[(\delta_2 + \delta_3) \cos \delta z - \frac{\delta_2 \delta_3 - 4QC}{(4QC)^{1/2}} \sin \delta z \right]^2 \tag{A.13}$$

Since Eq. A.12 may also be written as

$$\delta^2 - (\delta_2 + \delta_3)\,\delta + \delta_2 \delta_3 = 0 \tag{A.14}$$

we may write

$$\delta_2 + \delta_3 = -(\delta_1 + d + jb) \tag{A.15}$$

and

$$\frac{\delta_2 \delta_3 - 4QC}{(4QC)^{1/2}} = \frac{\delta_1 (\delta_1 + d + jb)}{(4QC)^{1/2}} \tag{A.16}$$

Thus we know the coefficients in Eq. A.13 and may calculate the maximum and minimum values of $f(QC,d,\delta z)$ and the angle at which a minimum occurs. These quantities are plotted in Figs. A.3, A.4, and A.5. These curves agree very well with those given by Watkins and further provide values of f for more closely spaced values of the parameter d.

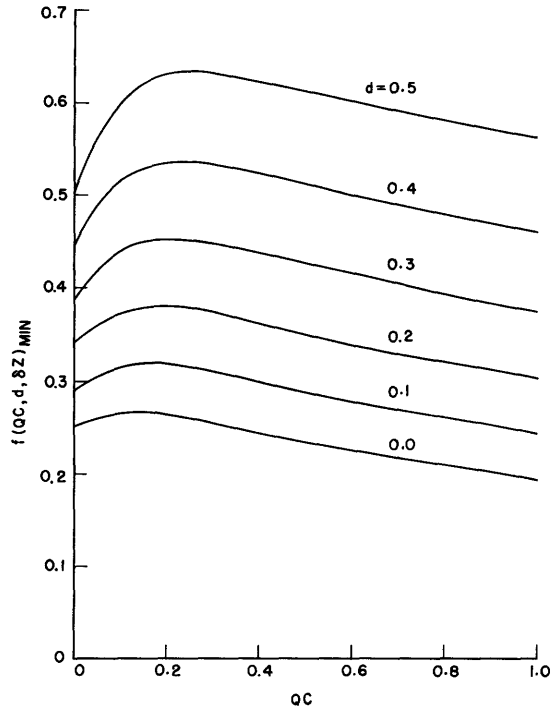

Fig. A.3
Graph of $f(QC, d, \delta z)_{min}$ vs QC with d as parameter.

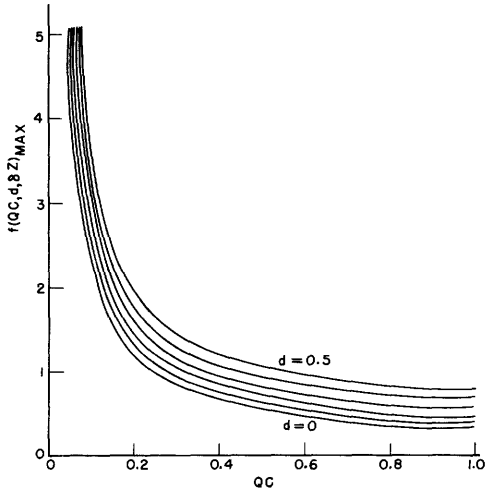

Fig. A.4
Graph of $f(QC, d, \delta z)_{max}$ vs QC with d as parameter.

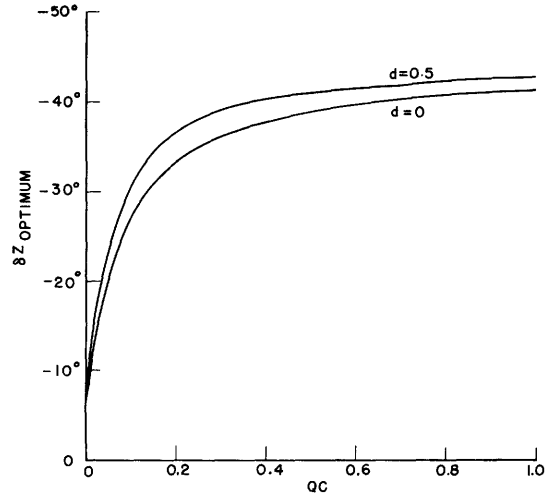

Fig. A.5
Graph of $\delta z_{optimum}$ vs QC with d as parameter.

TABLE A.1

y_1	x_1	QC	f(QC, d, δz) min	f(QC, d, δz) max	δz (degree)
d = 0					
−0.5	$\sqrt{0.75}$ = 0.86603	0.	0.25		0.
−0.5106	0.8600	0.0053	0.252	46.9	−7.17
−0.6	0.8147	0.0476	0.260	5.504	−20.23
−0.7	0.7726	0.0932	0.265	2.532	−20.23
−0.8	0.7365	0.1394	0.266	1.684	−30.20
−0.9	0.7046	0.1877	0.265	1.258	−32.76
−1.0	0.6761	0.2393	0.261	1.000	−34.64
−1.2	0.6269	0.3541	0.250	0.706	−37.20
−1.5	0.5679	0.5598	0.229	0.487	−39.45
−2.0	0.4963	0.9991	0.195	0.320	−41.42
d = 0.1					
−0.48805	0.8300	0.0032	0.291	81.99	−5.80
−0.5	0.8230	0.0089	0.292	30.04	−9.60
−0.6	0.7716	0.0544	0.308	4.767	−22.15
−0.7	0.7291	0.0983	0.315	2.607	−27.75
−0.8	0.6925	0.1433	0.319	1.794	−31.24
−0.9	0.6601	0.1908	0.318	1.366	−33.65
−1.0	0.6311	0.2417	0.315	1.102	−35.76
−1.2	0.5811	0.3556	0.304	0.795	−37.82
−1.5	0.5215	0.5605	0.281	0.563	−39.92
−1.995	0.4500	0.9944	0.245	0.384	−41.62
d = 0.2					
−0.4711	0.8000	0.0032	0.342	90.33	
−0.5	0.7827	0.0165	0.346	17.32	−13.39
−0.6	0.7312	0.0601	0.363	4.648	−23.78
−0.7	0.6885	0.1026	0.374	2.713	−28.94
−0.8	0.6515	0.1466	0.379	1.920	−32.20
−0.9	0.6188	0.1933	0.380	1.489	−34.46
−1.0	0.5895	0.2435	0.378	1.218	−36.10
−1.2	0.5390	0.3567	0.367	0.897	−38.36
−1.5	0.4792	0.5611	0.344	0.651	−40.35
−1.68	0.4500	0.7047	0.329	0.562	−41.11
−1.9785	0.4100	0.9782	0.306	0.463	−42.01

TABLE A.1 (continued)

y_1	x_1	QC	fmin	fmax	δz (degree)
d = 0.3					
−0.4587	0.7700	0.0047	0.390	65.85	−9.61
−0.5	0.7450	0.0231	0.403	13.22	−16.22
−0.6	0.6936	0.0649	0.426	4.634	−25.28
−0.7	0.6508	0.1061	0.442	2.848	−30.01
−0.8	0.6135	0.1492	0.450	2.066	−33.06
−0.9	0.58055	0.1951	0.452	1.629	−35.17
−1.0	0.5510	0.2450	0.451	1.348	−36.74
−1.2	0.5005	0.3575	0.442	1.013	−38.86
−1.448	0.4500	0.5230	0.425	0.783	−40.48
−1.764	0.4000	0.7774	0.396	0.622	−41.72
−2.000	0.3700	0.9997	0.377	0.544	−42.34
d = 0.4					
−0.4504	0.74	0.0075	0.449	44.04	−9.79
−0.5	0.7099	0.0286	0.470	11.40	−18.45
−0.6	0.6586	0.0688	0.499	4.704	−26.56
−0.7	0.6157	0.1090	0.519	3.000	−30.98
−0.8	0.5783	0.1512	0.530	2.231	−33.83
−0.9	0.5452	0.1967	0.536	1.783	−35.84
−1.0	0.5157	0.2461	0.536	1.493	−37.31
−1.2	0.4653	0.3581	0.528	1.143	−39.32
−1.270	0.45	0.4017	0.524	1.060	−39.81
−1.537	0.4	0.5899	0.502	0.844	−41.23
−1.889	0.35	0.8918	0.472	0.682	−42.32
−1.973	0.34	0.9730	0.465	0.655	−42.52
d = 0.5					
−0.4307	0.7200	0.0047	0.509	75.11	−8.04
−0.5	0.6771	0.0333	0.543	10.44	−20.33
−0.6	0.6261	0.0722	0.581	4.821	−27.73
−0.7	0.5831	0.1114	0.607	3.191	−31.86
−0.8	0.5457	0.1529	0.622	2.412	−34.54
−0.9	0.5127	0.1979	0.631	1.954	−36.43
−1.0	0.4832	0.2469	0.634	1.654	−37.82
−1.128	0.45	0.3162	0.631	1.396	−39.14
−1.361	0.4	0.4623	0.617	1.109	−40.73
−1.663	0.35	0.6911	0.592	0.901	−41.96
−1.979	0.31	0.9790	0.564	0.772	−42.76

ACKNOWLEDGMENT

I wish to express my sincere gratitude to Mr. L. D. Smullin for his highly valued advice during this project. Thanks are also due to Professor L. J. Chu for his help and encouragement; to Mr. H. A. Haus, who is largely responsible for the derivation in Section II on the "Potential Distribution in the Beam;" and to Mr. L. Stark and Mr. H. E. Rowe for many helpful discussions.

References

1. D. A. Watkins: Noise Reduction in Beam Type Amplifiers, Electronics Research Laboratory, Stanford University Technical Report No. 31, March 1951

2. R. W. Peter: Investigation on Noise in Long Electron Beams, talk given at the Tenth Annual Conference on Electron Tubes, Ottawa, Canada, June 17, 1952

3. J. R. Pierce: Theory and Design of Electron Beams, Van Nostrand, New York, 1949

4. L. M. Field, K. Spangenberg, R. Helm: Control of Electron Beam Dispersion at High Vacuum by Ions, Elec. Comm. 24, 108-121, 1947

5. J. T. Tate, P. T. Smith: The Efficiencies of Ionization and Ionization Potentials of Various Gases Under Electron Impact, Phys. Rev. 39, 270-277, 1932

6. F. B. Llewellyn: Electron Inertia Effects, Cambridge University Press, Cambridge, England, 1941

7. F. B. Llewellyn, L. C. Peterson: Vacuum Tube Networks, Proc. I.R.E. 32, 133-166, 1944

8. W. C. Hahn: Small Signal Theory of Velocity Modulated Electron Beams, Gen. Elec. Rev. 42, 258-270, 1939

9. S. Ramo: Space Charge and Field Waves in an Electron Beam, Phys. Rev. 56, 276, 1939

10. C. C. Cutler, C. F. Quate: Experimental Verification of Space Charge and Transit Time Reduction of Noise in Electron Beams, Phys. Rev. 80, 875-878, 1950

11. P. Parzen: Space Charge Wave Propagation in a Cylindrical Electron Beam of Finite Lateral Extension, J. Appl. Phys. 23, 215, 1952

12. L. D. Smullin: Propagation of Disturbances in One Dimensional Accelerated Electron Streams, J. Appl. Phys. 22, 1496-1498, 1951

13. H. A. Haus: Standing Wave Pattern of Noise Current in Presence of a Velocity Distribution, unpublished report, Research Laboratory of Electronics, M.I.T., Feb. 5, 1952

14. J. R. Pierce: Traveling-Wave Tubes, Van Nostrand, New York, 1950

15. H. E. Rowe: Shot Noise in Electron Beams, Technical Report No. 239, Research Laboratory of Electronics, M.I.T., 1952